Engineering Fracture Mechanics 148 (2015) 134–144

Contents lists available at ScienceDirect

Engineering Fracture Mechanics

journal homepage: www.elsevier.com/locate/engfracmech

Evaluation of the fracture toughness of brittle hardening materials by Vickers indentation

Felix Rickhey [a], Karuppasamy Pandian Marimuthu [a], Jin Haeng Lee [b], Hyungyil Lee [a,*], Jun Hee Hahn [c]

[a] Sogang University, Department of Mechanical Engineering, Seoul 121-742, Republic of Korea
[b] Research Reactor Mechanical Structure Design Division, Korea Atomic Energy Research Institute, Daejeon 305-353, Republic of Korea
[c] Division of Industrial Metrology, Korea Research Institute of Standards and Science, Daejeon 305-340, Republic of Korea

ARTICLE INFO

Article history:
Received 10 April 2015
Received in revised form 5 September 2015
Accepted 8 September 2015
Available online 15 September 2015

Keywords:
Fracture toughness
Strain hardening
Indentation cracking
Finite element analysis
Cohesive zone model

ABSTRACT

We propose a Vickers indentation cracking-based method for evaluating the fracture toughness of brittle materials exhibiting strain hardening. The approach is an extension of the recent method by Hyun et al. (2015) for non-hardening materials to hardening materials. The hardening material is simplified by an equivalent non-hardening material with an elevated modified yield strain so that the fracture toughness of a hardening material can be evaluated with the formula proposed by Hyun et al. The proposed extension is verified by comparison with experimental results from nanoindentation tests on Ge(100) and Si(100).

1. Introduction

The fracture toughness K_c, which describes the resistance to crack growth, is an important parameter in the reliability assessment of structures. Traditional test methods for fracture toughness evaluation are well standardized, but specimen fabrication and testing are tedious and expensive. A fast, simple and inexpensive method with minimum specimen preparation, the sharp indentation test represents yet another potential way to evaluate the fracture toughness of brittle materials. Here, it is made use of the final length c of the cracks that have initiated at the surface (radial crack) or inside the material (median crack) and have grown to full size (radial-median crack or half-penny crack) during unloading, where it is driven by the increasing mismatch between the contracting outer elastic matrix and the inner, nearly rigid, plastic zone (Fig. 1). However the indentation-based method lacks in terms of accuracy due to an insufficient understanding of the complex relation between the crack and the simultaneously evolving stress field under the indenter, which depends on material properties, indentation load (or depth) and indenter shape.

To establish and improve the sharp indentation method, numerous studies were conducted in the late 1970s [1–3], culminating in the often-applied equation suggested by Lawn et al. [4], who provided a link between the stress field and the fracture mechanics side of the problem. Accordingly, the fracture toughness K_c was calculated from Young's modulus E, hardness H, the maximum indentation load P_{max}, and crack length c (Fig. 1) as follows

* Corresponding author. Tel.: +82 2 705 8636; fax: +82 2 712 0799.
E-mail address: hylee@sogang.ac.kr (H. Lee).

http://dx.doi.org/10.1016/j.engfracmech.2015.09.028
0013-7944/

Nomenclature

a	impression half-diagonal
c	crack length measured on surface
E	Young's modulus
E_R	Young's modulus ratio (E/1000 GPa)
h	indentation depth
H	hardness
K_c	fracture toughness (mode I)
n	strain hardening coefficient
P_{max}	maximum indentation load
α	correction factor
Γ	fracture energy
δ_c	crack-initiating separation
δ_{max}	damage-initiating separation
ε_o	(initial) yield strain
ε_{om}	modified (initial) yield strain
κ_h	correction factor (hardening material)
κ_{nh}	correction factor (non-hardening material)
ν	Poisson's ratio
σ_{max}	damage-inducing stress threshold
σ_o	(initial) yield stress

$$K_c = \alpha\left(\frac{E}{H}\right)^{1/2}\left(\frac{P_{max}}{C^{3/2}}\right) \tag{1}$$

The coefficient α was initially introduced to account for the indenter shape represented by the number of edges and indenter angle ψ. Fitting experimental data for diverse brittle materials, Anstis et al. [5] found $\alpha = 0.016 \pm 0.004$. Eq. (1) has been the basis of most subsequent studies on indentation cracking [6–9], and a number of modified formulations have emerged (e.g. [10–12]; see [13] for a detailed discussion). However, studies also revealed that Eq. (1) lacks accuracy due to an oversimplified stress field (for instance, the comparison of the sub-indenter stress field to a pressurized cavity means a neglect of the free specimen surface and associated pile-up/sink-in) and, as a consequence, application of Eq. (1) may lead to inaccurate K_c values.

Many attempts have been made since then to account for the influence of material properties and the indenter shape. Jang and Pharr [14] carried out indentation tests on single-crystalline Ge(100) and Si(100) using 3-sided pyramidal indenters of diverse angles ψ; based on the derivation of Eq. (1) outlined in [4] an attempt was made to include the influence of Poisson's ratio ν in the formulation. Lee et al. [15] simulated Vickers indentation cracking by using the cohesive zone model (CZM). Finite element (FE) results were in a good agreement with the experimental observations made by Lawn et al. [4]. Making use of the proportionality $P_{max} \propto c^{3/2}$, Hyun et al. [16,17] recently extended the study and suggested a fracture toughness equation, which takes into account E, ν, yield strain ε_o, which replaces H, as well as ψ and the number of indenter edges. The material was assumed to be elastic-perfectly plastic and $\varepsilon_o = \sigma_o/E$ was estimated by varying σ_o until the hardness from FE

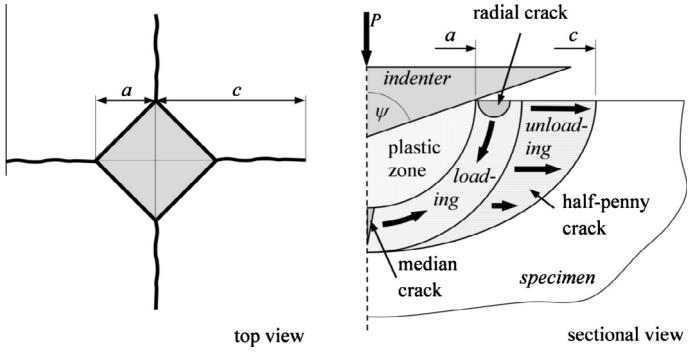

Fig. 1. Schematic figure of radial-median cracking under a quadrangular pyramidal indenter.

analysis matched the measured H value. Resulting K_c values showed some deviation from the values obtained by standardized test methods, which was presumably in part due to errors inherent in the problematic parameter H, deduced from the contact diagonal $2a$ and the neglect of hardening. Apart from the load-depth (P–h) curve and c, accurate knowledge of material properties is thus crucial for the evaluation of K_c.

In this paper, we extend the fracture toughness equation of Hyun et al. [17] for non-hardening materials by accounting for the influence of hardening. To reduce the computational and post-processing efforts, we propose a simplified *equivalent* non-hardening model, where the hardening material is interpreted as a non-hardening material with an elevated modified yield strain, which is then inserted in the equation established for non-hardening materials. Finally, indentation experiments are conducted on Si(100) and Ge(100) and the K_c values obtained by our suggested method are compared with literature values. To obtain the material properties of Si(100) and Ge(100), a recently established spherical indentation-based material property evaluation method by Kim et al. [18] is applied.

2. FE analysis of indentation cracking

2.1. FE model for indentation cracking

For the simulation of Vickers indentation cracking, the commercial software Abaqus/Standard is used. The FE model is shown in Fig. 2. Considering geometrical and loading symmetry, modeling of a quarter section of the specimen is sufficient. The model consists of about 86,600 elements and 97,000 nodes. Apart from those elements adjacent to the symmetry (= loading) axis, where we use 6-node brick elements, 8-node first order brick elements are used. Fully integrated elements are employed due to their good compatibility with the cohesive elements and their good convergence in cracking analysis. Details on the selection of the element type are given in the Appendix.

Cohesive elements (COH3D8 [19]) are placed in median planes, where the crack is expected to initiate and propagate during indentation. Their behavior is governed by a traction-separation law. Since the shape of the traction-separation curve is only of secondary importance [20], a bilinear traction-separation curve is assumed for convenience. Damage initiates when the tensile stress normal to the median plane meets a damage initiation stress σ_{max}. Upon further loading the element gradually loses its stiffness according to the damage model. The element cracks, *i.e.* loses its entire stiffness, once the accumulated damage energy reaches the critical fracture energy, which is tantamount to reaching the critical separation δ_c. The area under the traction-separation curve is equal to the fracture energy Γ. The material fracture toughness K_c is given through

$$\Gamma = \frac{K_c^2}{E'} = \frac{1}{2}\sigma_{max}\delta_c; \quad E' = \begin{cases} E & \text{for plane stress} \\ E/(1-\nu^2) & \text{for plane strain} \end{cases} \tag{2}$$

The stress–strain relationship is expressed by the power-law hardening material model proposed by Hollomon

$$\frac{\varepsilon}{\varepsilon_o} = \begin{cases} \frac{\sigma}{\sigma_o} & \text{for } \sigma \le \sigma_o \\ \left(\frac{\sigma}{\sigma_o}\right)^n & \text{for } \sigma > \sigma_o;\ 1 < n \le \infty \end{cases} \tag{3}$$

where σ_o, ε_o and n are initial yield strength, yield strain, and strain hardening exponent, respectively. The material shows hardening behavior when the strain hardening exponent is between $1 < n < \infty$, while $n = \infty$ represents the elastic-perfectly plastic case.

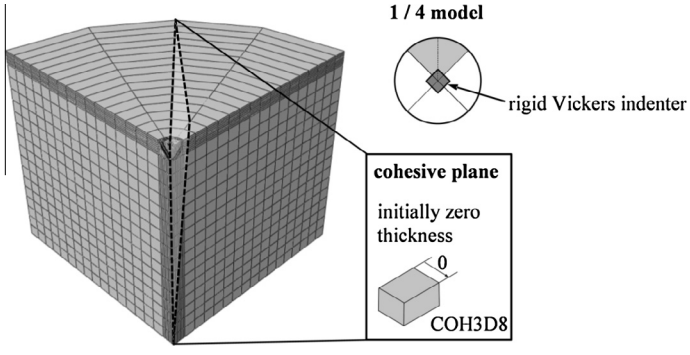

Fig. 2. FE model for Vickers indentation cracking analysis using cohesive elements.

2.2. Determination of the maximum indentation depth necessary for well-developed cracks

The indentation cracking-based method for evaluating K_c makes use of the observation that $P_{max}/c^{3/2}$ reaches a constant value for a sufficiently large maximum indentation depth h_{max} (or load P_{max}). This means that beyond a minimum h_{max} that provides the formation of a well-developed crack, denoted h^*_{max}, the parameter $\kappa|_{FE}$ [$= K_c/(P_{max}/c^{3/2})$] becomes independent of P_{max} and the crack has then assumed the characteristic well-developed half-penny shape.

Since the single influences of E, ε_o and n on the final crack lengths cannot be simply predicted from Eq. (1), FE analysis is used to provide insight into the particular roles of E, ε_o and n. Further, as application of Eq. (1) requires well-developed cracks, results are also used to determine h^*_{max}. In the following the material properties ν (= 0.3), Γ (= 0.0025 GPa μm) are kept constant, while either E, ε_o, or n are varied. Fig. 3 shows the crack shapes at the unloaded state for combinations of E = 100, 200 GPa, ε_o = 0.02, 0.1 ($n = \infty$) and h_{max} = [0.6, 1.4] μm. h^*_{max} increases as E and ε_o decrease. For E = 100 GPa and ε_o = 0.02, well-developed cracks form at $h_{max} \geqslant 1.4$ μm. However, for E > 100 GPa and ε_o > 0.02, well-developed cracks form at a lower h_{max} < 1.0 μm. Fig. 4 shows the influence of the strain hardening coefficient n (= 5, 13) on the final crack. From Figs. 3(a) and 4(a)–(b), we find that h^*_{max} increases as n decreases. Fig. 5 shows the corresponding relations between $P_{max}/c^{3/2}$ and h_{max}. For the materials with E = 200 GPa and ε_o = 0.02, $P_{max}/c^{3/2}$ decreases with increasing h_{max} monotonically to a constant value, while for the materials with E = 100 GPa and ε_o = 0.02, $P_{max}/c^{3/2}$ we observe some fluctuation even for high h_{max}. We conclude that apart from the materials with E = 100 GPa and ε_o = 0.02, which is not treated hereafter, well-developed cracks form at indentation depths $h_{max} \geqslant 1.0$ μm for all hardening and non-hardening materials. To avoid unnecessarily high computational costs and provide sufficiently high mesh density, the maximum indentation depth is therefore set to h_{max} = 1.0 μm.

3. Evaluation of the fracture toughness of hardening materials using a modified yield strain

To improve the accuracy of Eq. (1), Hyun et al. [17] defined a parameter κ_{nh} – the subscript nh refers to non-hardening –, in which influences from properties of an isotropic non-hardening material (E, ε_o, ν) were merged. The fracture toughness equation was then reformulated as

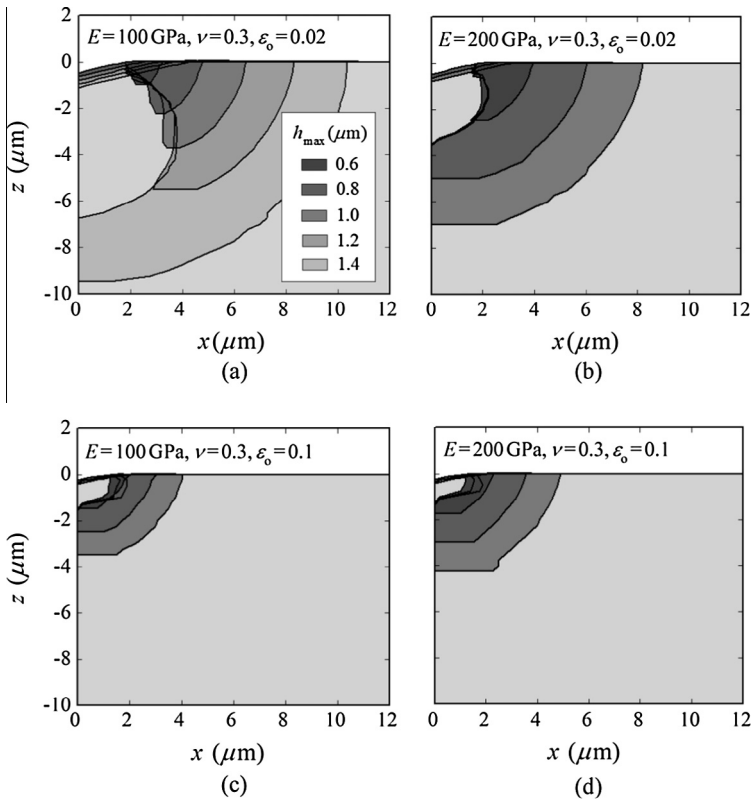

Fig. 3. Variation of crack shapes with h_{max} after unloading for non-hardening materials ($n = \infty$) for diverse combinations of E and ε_o; half-penny crack occurs at h_{max} = 1.4 (a), 0.8 (b, c), 0.6 μm (d), respectively.

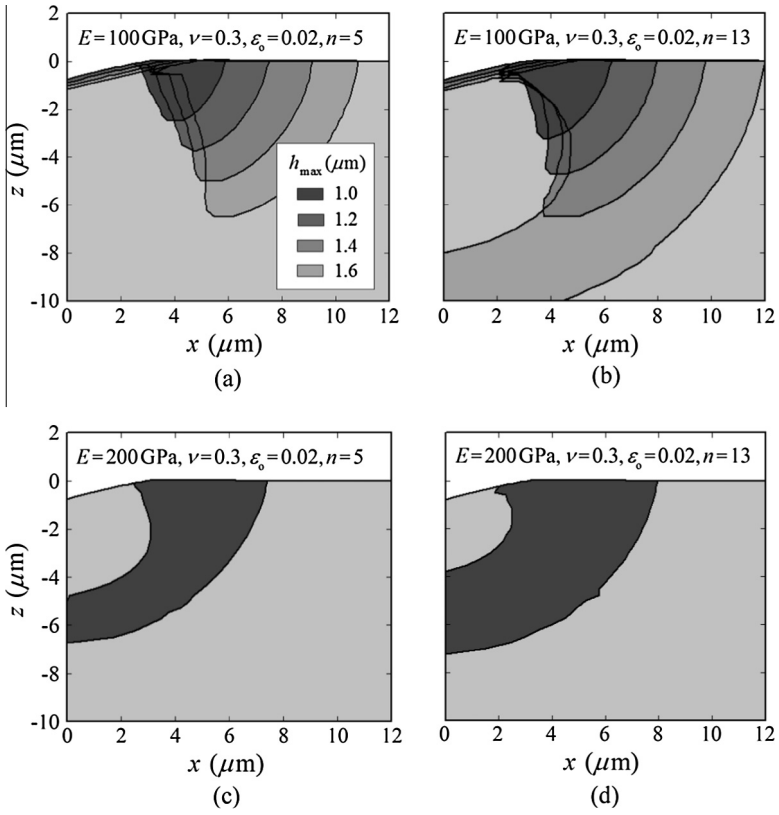

Fig. 4. Change of crack shape with h_{max} after unloading for diverse combinations of E and n.

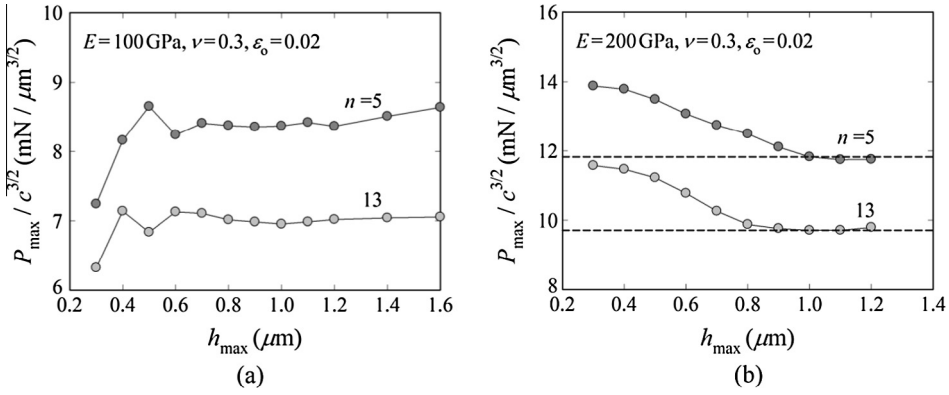

Fig. 5. $P_{max}/c^{3/2}$ vs. h_{max} for (a) E = 100 and (b) 200 GPa (ν = 0.3, ε_o = 0.02).

$$K_c = \kappa_{nh}(E_R, \varepsilon_o, \nu)\left(\frac{P_{max}}{c^{3/2}}\right) \tag{4}$$

where E_R is the ratio of the Young's modulus to a reference value, E = 1000 GPa ($\equiv E_{1000}$), *i.e.* $E_R \equiv E/E_{1000}$, to make κ_{nh} dimensionless. Varying K_c, E, ε_o, ν, a relation between κ_{nh} and material properties was established by regression.

To consider strain hardening, we could expand the function in Eq. (4) by n, which would make κ_h (subscript h for hardening) a function of four variables E, ε_o, ν and n. To avoid extensive numerical analysis this direct approach would entail and to obviate the establishment of a new fracture toughness equation, we assume a simplified *equivalent* non-hardening material instead of a hardening material as shown in Fig. 6 so that Eq. (4) is still applicable. The equivalent non-hardening material is defined as follows. The gray and the black solid lines in Fig. 6, represent the original hardening material, characterized by ε_o and n, and the equivalent non-hardening material, characterized by the modified yield strain ε_{om}, respectively.

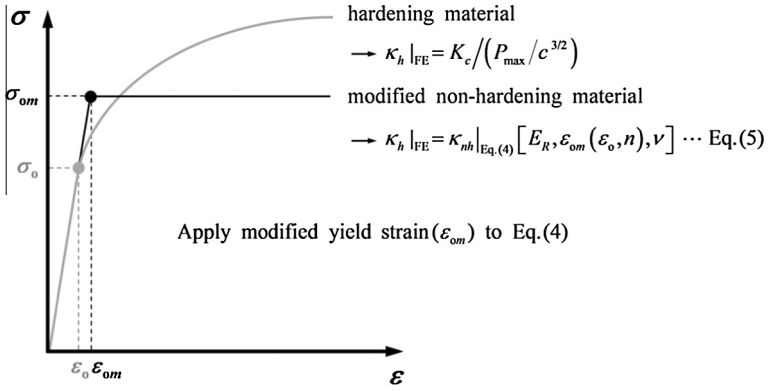

Fig. 6. Stress–strain curves for hardening and simplified equivalent non-hardening materials.

To obtain ε_{om}, we first perform Vickers indentation cracking analyses for the *hardening* material (E, ν, ε_o, n) with given K_c and extract maximum indentation load P_{max} and crack length c; then we get $\kappa_h|_{FE}$ from the definition of κ as $\kappa_h|_{FE} = K_c/(P_{max}/c^{3/2})$ (subscript h for hardening). Second, this $\kappa_h|_{FE}$ is set to be equal to $\kappa_{nh}|_{Eq.\,(4)}$ for the equivalent *non-hardening* material with ε_{om} (and equal E and ν), *i.e.*

$$\kappa_h|_{FE} = \kappa_{nh}|_{Eq.\,(4)}(E_R, \varepsilon_{om}, \nu) \tag{5}$$

Solving the above equation gives the value of modified yield strain ε_{om}.

We determine the main variables that affect the modified yield strain ε_{om} by the Taguchi method [21]. The orthogonal array L$_9$ (3^4) is used for four factors (E, ν, ε_o, n) with the three levels. The ranges of E, ν, ε_o are equal to the ranges in Hyun et al. [17]. For n we use values >5, which covers the range of common materials. Based on the orthogonal array, the effect of each variable (E, ν, ε_o, n) on ε_{om} is evaluated with 9 combinations of factor and level. As a result, it is found that the variables ε_o and n have a much larger effect on ε_{om} than E and ν have. Details of this procedure is omitted here, but the finding is verified as follows. For fixed E = 200 GPa, ν = 0.3, the values of ε_o and n are varied (ε_o: 5 × n: 7). Fig. 7 shows the variation of ε_{om} for different combinations of ε_o and n (marked with symbols); thus ε_{om} can be expressed as a function of ε_o and n. For combinations of (fixed) ε_o = 0.02, 0.1 and n = 5, 13, the values of E and ν are varied (E: 4 × ν: 4). In Fig. 8, ε_{om} is constant for equal ε_o and n, regardless of E and ν These results are consistent with the finding of Lee et al. [22,23], in which n and ε_o (not the absolute values σ_o and E themselves but the ratio $\varepsilon_o = \sigma_o/E$) are the only variables governing the indentation characteristics. In brief, we consider only ε_o and n to express ε_{om}.

Regressing the data in Fig. 7 to a 2nd order polynomial, ε_{om} can be expressed as a function of ε_o and n as

$$\begin{aligned} \varepsilon_{om}(\varepsilon_o, n) &= a_i(\varepsilon_o) n^{-i}; \quad i = 0,1,2 \\ a_i(\varepsilon_o) &= b_{ij}\,\varepsilon_o^j; \quad j = 0,1,2,3 \end{aligned} \tag{6}$$

Table 1 lists the regression coefficients b_{ij}. The regression curves of Eq. (6) plotted in Figs. 7 and 8 (solid lines) agree well with the FE data (white symbols; n = 3, 7, ∞) and also with the data not considered in the regression (gray symbols; n = 4, 5, 10, 20). The fracture toughness can then be calculated by substituting ε_{om} for ε_o in Eq. (4), *i.e.*

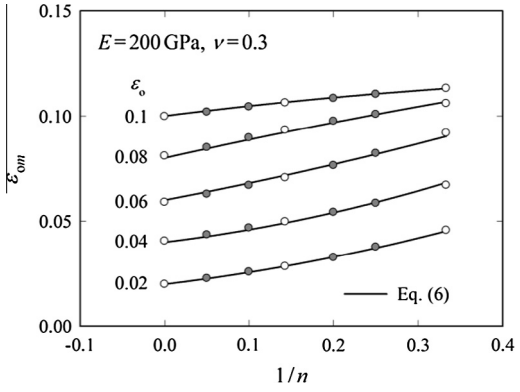

Fig. 7. ε_{om} vs. $(1/n)$ curves for six different ε_o.

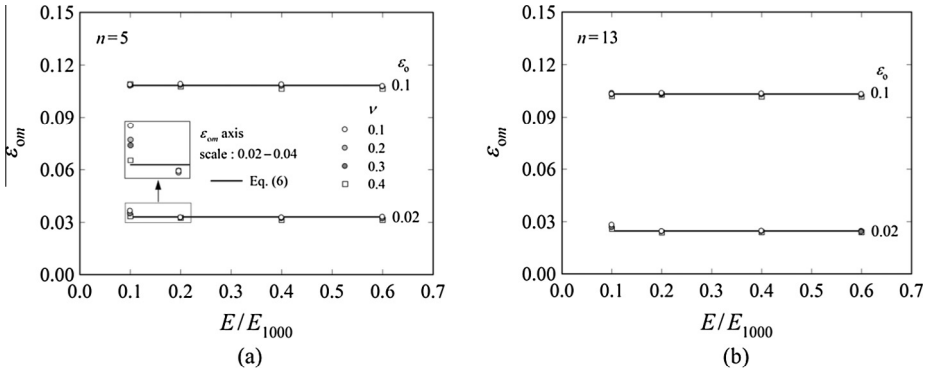

Fig. 8. ε_{om} vs. E/E_{1000} data for (a) $n = 5$, (b) $n = 13$; radial cracks occur when $E = 100$ GPa and $\varepsilon_o = 0.02$ for $n = 5$, 13.

Table 1
Coefficients b_{ij} of Eq. (6).

	$i = 0$	$i = 1$	$i = 2$
$j = 0$	1.052e−3	1.231e−1	−1.342e−1
$j = 1$	9.849e−1	−6.529e+0	1.668e+1
$j = 2$	0	1.529e+2	−3.372e+2
$j = 3$	0	−9.472e+2	1.799e+3

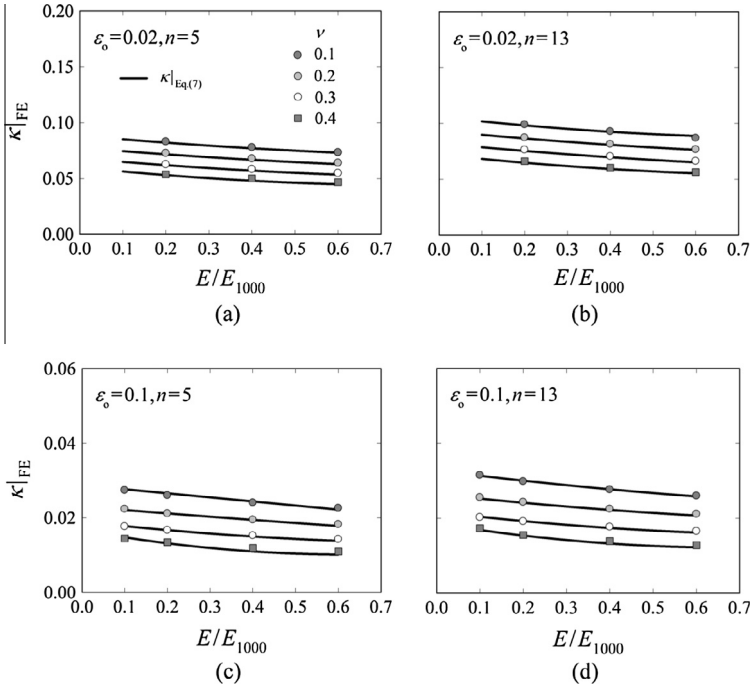

Fig. 9. Comparison of $\kappa|_{FE}$ data with regression curves of $\kappa|_{Eq.\ (7)}$ for various values of E and ν.

$$K_c = \kappa_{nh}(E_R, \varepsilon_{om}, \nu)\left(\frac{P_{max}}{c^{3/2}}\right) \tag{7}$$

where ε_{om} is given in Eq. (6).

Varying E and ν, indentation cracking analyses are conducted for all combinations of $\varepsilon_o = 0.02$, 0.1 and $n = 5$, 13. Comparing FE values for $\kappa|_{FE}$ [$= K_c/(P_{max}/c^{3/2})$] with those from Eq. (7), $\kappa|_{Eq.\ (7)}$, we find from Fig. 9 that Eq. (7) is also valid for materials with different E and ν, although it was derived using fixed values ($E = 200$ GPa, $\nu = 0.3$). Note that by using the simplified

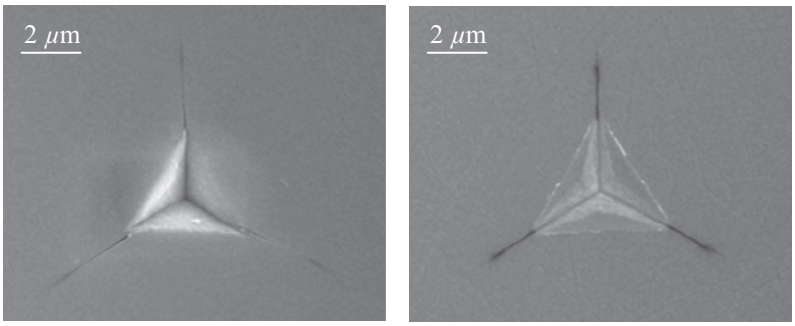

Fig. 10. SEM micrographs for Si(100) and Ge(100) after indentation to P_{max} = 50 mN.

Table 2
P_{max} and c from Berkovich nano-indentation test.

Material	Indenter	P_{max} (mN)	c (μ m)
Si(100)	Berkovich	50	2.48
	Vickers (converted)		2.25
Ge(100)	Berkovich	50	3.26
	Vickers (converted)		2.99

Table 3
Material properties from spherical nano-indentation test.

Material	E (GPa) [24]	σ_o (MPa)	n
Si(100)	130	2.6	2.8
Ge(100)	104	3.1	4.0

Table 4
Comparison of fracture toughness values from indentation and conventional methods.

Material	K_c (MPa m$^{1/2}$)		
	Conventional method	Indentation-based methods	
	Jaccodine [25]; DCB[a]	Previous (deviation, %)	Eq. (7) (deviation, %)
Si(100)	0.76	Hyun et al. [17] 0.82 (+8%)	0.77 (+1%)
Ge(100)	0.63	Lemaitre [26] 0.53 ± 0.06 (−16 ± 10%)	0.53 (−16%)

[a] DCB (double cantilever beam): K_c from surface energies γ.

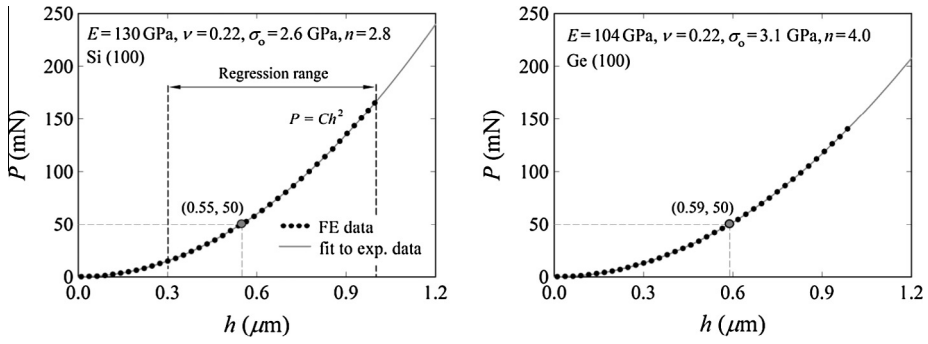

Fig. 11. Load-depth curves for Si(100) and Ge(100).

Table 5
c values from nano-indentation tests and FE analyses for Si(100) and Ge(100); P_{max} = 50 mN.

Material	K_c (MPa m$^{1/2}$)	Crack length c (μm)		Deviation (%)
		Nano-indentation test	FEA	
Si(100)	0.77	2.48	2.33	6.0
Ge(100)	0.53	3.26	3.12	4.3

equivalent non-hardening material model, the number of FE analysis required to propose a toughness evaluation method for hardening materials could be reduced significantly.

4. Validation of property evaluation approach by nano-indentation tests

To assess the proposed evaluation method the fracture toughnesses of Si(100) and Ge(100) are predicted by Eq. (7) and compared to values from the literature. Indentation tests with Berkovich indenter are performed on a nano-indenter (Nano indenter® XP, Agilent Technologies). The applied load is set to P_{max} = 50 mN. Tests are carried out with a constant loading and unloading rate of 0.5 mN/s. The radial crack length c is measured after unloading from SEM (scanning electron microscope) images. The mean average of the lengths of the three cracks is taken as c.

Although Eq. (7) is established for Vickers indentation, we use the Berkovich indenter, which is usually preferred in nano-indentation tests owing to the difficulties associated with the manufacturing of Vickers nano-indenters. The main difference between these two indenters is the resulting number of cracks and the crack size. The ratio of the crack lengths c_B and c_V produced by Berkovich and Vickers indenters, respectively, was found to be $c_B/c_V \approx 1.10$ [16]. Crack patterns for Si(100) and Ge(100) after indentation to P_{max} = 50 mN are shown in Fig. 10; crack lengths c are listed in Table 2. Material properties of Si(100) and Ge(100), required for the determination of K_c, were recently determined by Kim et al. [18] and are provided in Table 3.

K_c values obtained by the proposed method are compared with the corresponding surface energies γ evaluated by Jaccodine [25]. Using DCB (double cantilever beam) specimens, Jaccodine found γ = 0.0213 and 0.0184 J/mm^2 for Si(100) and Ge(100), respectively. K_c is related to γ by

$$K_c = \left(\frac{E\Gamma}{1-\nu^2}\right)^{1/2}; \quad \Gamma = 2\gamma \tag{8}$$

which yields K_c = 0.76 and 0.63 MPa m$^{1/2}$ for Si(100) and Ge(100), respectively. These reference values are compared in Table 4 with indentation-based results by Hyun et al. [17], Lemaitre [25] and those calculated using Eqs. (6) and (7). K_c values obtained by Hyun et al. [17] and Lemaitre [26], both of who did not account for potential strain hardening, deviate by 8% and 16 ± 10% for Si and Ge, respectively; using Eqs. (6) and (7), the respective deviations are 1% and 16%. Note that Lemaitre [26] determined K_c with α = 0.016 [5] in Eq. (1).

For further validation of our approach, FE indentation cracking analyses are run with the material properties of Si(100) and Ge(100) in Tables 3 and 4 to directly compare resulting crack lengths. Since we observed in FE indentation cracking analysis better convergence with a prescribed displacement than with a prescribed load, we first determine the h_{max} values corresponding to the experimental load P_{max} = 50 mN by fitting the FE load-depth (P–h) curves of the two materials (dotted lines in Fig. 11) to the theoretical relation $P = Ch^2$ (thin solid lines); h_{max} = 0.55 μm for Si(100) and 0.59 μm for Ge(100). The FE analyses with these h_{max} values give crack lengths that deviate by only 6% [Si(100)] and 4.3% [Ge(100)] from those measured in the real nano-indentation test (Table 5).

5. Conclusions

Based on FE analyses, we presented a Vickers indentation-based method for determining the fracture toughness of brittle materials that exhibit strain hardening behavior. Damage and cracking was simulated by using cohesive elements in the median planes of expected radial-median cracking. For simplicity and to reduce computational costs, the hardening material was interpreted as a non-hardening material with a modified yield strain. The modified yield strain ε_{om} was expressed as a function of yield strain ε_o and hardening coefficient n, both of which were found to be the parameters governing ε_{om}. The fracture toughness K_c was then obtained by replacing ε_o with ε_{om} in the equation for non-hardening materials, recently established by Hyun et al. [17]. Necessary material properties were determined from the spherical indentation load-depth curve.

Indentation experiments were conducted on mono-crystalline Si(100) and Ge(100). The suggested method gave equal or improved agreement with K_c values obtained with DCB specimens from the literature than earlier indentation approaches neglecting hardening.

Acknowledgement

This research was supported by Basic Science Research Program through the National Research Foundation of Korea (No. NRF-2012 R1A2A2A 01046480).

Appendix A. Determination of element type for Vickers indentation simulation

The element type used in the FE model for Vickers indentation cracking is chosen based on the comparison of the crack shapes obtained with diverse element types. Abaqus [19] provides only cohesive elements of first order. To avoid difficulties that arise when connecting first order to higher order elements, 8-node brick elements are used for the specimen. To compensate for the (low) first-order interpolation and to sufficiently capture small deformations, elements of edge length 0.25 μm are deployed in the very vicinity to the contact.

We compare the crack shapes obtained with elements using full (C3D8; [19]) and reduced integration (C3D8R). Fig. A1(a) for C3D8 and A1(b) for C3D8R depict the cracks after unloading. With C3D8R elements we observe that crack faces are heavily distorted, which means that the crack length cannot be measured accurately. Further, the use of these elements affects convergence in a negative way and even increases the analysis time (if convergence is reached). The use of C3D8 elements is therefore recommended.

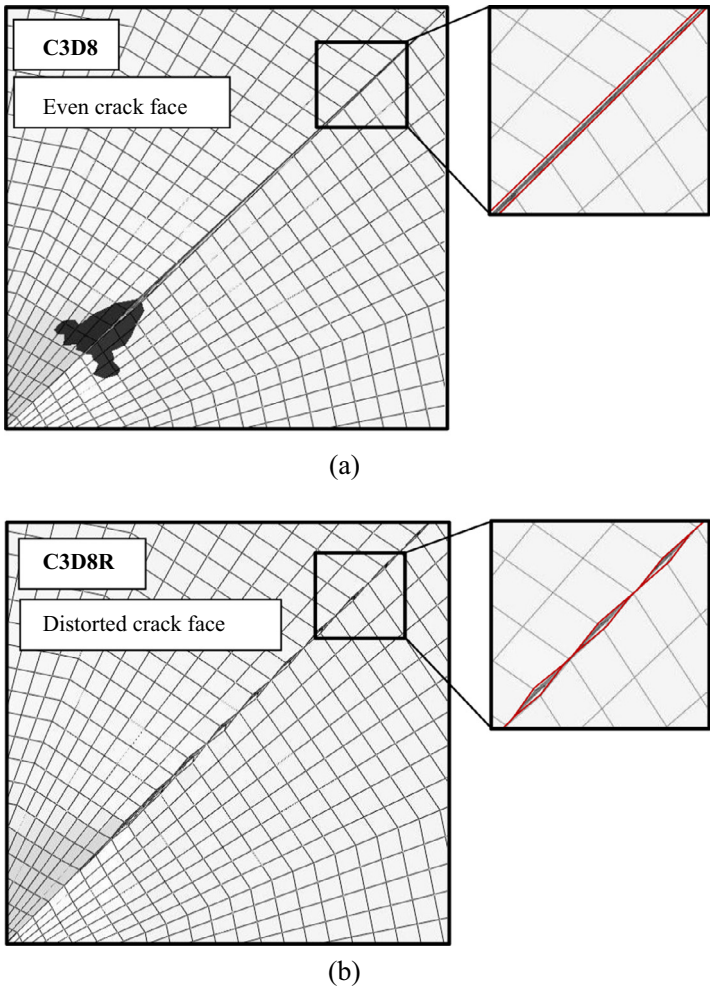

Fig. A1. Crack appearance on surface after unloading for (a) C3D8 elements, (b) C3D8R elements.

References

[1] Lawn BR, Wilshaw TR. Indentation fracture: principles and applications. J Mater Sci 1975;10:1049–81.
[2] Evans AG, Charles EA. Fracture toughness determinations by indentation. J Am Ceram Soc 1976;59:371–2.
[3] Lawn BR, Evans AG. A model for crack initiation in elastic/plastic indentation fields. J Mater Sci 1977;12:2195–9.
[4] Lawn BR, Evans AG, Marshall DB. Elastic/plastic indentation damage in ceramics: the median/radial crack system. J Am Ceram Soc 1980;63:574–81.
[5] Anstis GR, Chantikul P, Lawn BR, Marshall DB. A critical evaluation of indentation techniques for measuring fracture toughness: I, direct crack measurements. J Am Ceram Soc 1981;64:533–8.
[6] Chiang SS, Marshall DB, Evans AG. The response of solids to elastic/plastic indentation. I. Stresses and residual stresses. J Appl Phys 1982;53:298–311.
[7] Chiang SS, Marshall DB, Evans AG. The response of solids to elastic/plastic indentation. II. Fracture initiation. J Am Ceram Soc 1982;53:312–7.
[8] Tanaka K. Elastic/plastic indentation hardness and indentation fracture toughness: the inclusion core model. J Mater Sci 1987;22:1501–8.
[9] Burghard Z, Zimmermann A, Rödel J, Aldinger F, Lawn BR. Crack opening profiles of indentation cracks in normal and anomalous glasses. Acta Mater 2004;52:293–7.
[10] Niihara K, Morena R, Hasselman DPH. Evaluation of K_{Ic} of brittle solids by the indentation method with low crack-to-indent ratios. J Mater Sci Lett 1982;1:13–6.
[11] Lankford J. Indentation microfracture in the Palmqvist crack regime: implications for fracture toughness evaluation by the indentation method. J Mater Sci Lett 1982;1:493–5.
[12] Laugier MT. The elastic/plastic indentation of ceramics. J Mater Sci Lett 1985;4:1539–41.
[13] Ponton CB, Rawlings RD. Vickers indentation fracture toughness test Part 1. Review of literature and formulation of standardised indentation toughness equations. *Mater Sci Tech* 1989;5:865–72.
[14] Jang J-i, Pharr GM. Influence of indenter angle on cracking in Si and Ge during nano-indentation. Acta Mater 2008;56:4458–69.
[15] Lee JH, Gao Y, Johanns KE, Pharr GM. Cohesive interface simulations of indentation cracking as a fracture toughness measurement method for brittle materials. Acta Mater 2012;60:5448–67.
[16] Hyun HC, Rickhey F, Lee JH, Hahn JH, Lee H. Characteristics of indentation cracking using cohesive zone finite element techniques for pyramidal indenters. Int J Solids Struct 2014;51:4327–35.
[17] Hyun HC, Rickhey F, Lee JH, Kim M, Lee H. Evaluation of indentation fracture toughness for brittle materials based on the cohesive zone finite element method. Engng Fract Mech 2015;134:304–16.
[18] Kim M, Marimuthu KP, Lee JH, Lee H. Spherical indentation method to evaluate material properties of high-strength materials. Int J Mech Sci 2015 [submitted for publication].
[19] Abaqus (v6.12). User's Manual. Providence, RI: Dassault Systèmes; 2012.
[20] Hutchinson JW, Evans AG. Mechanics of materials: top-down approaches to fracture. Acta Mater 2000;48:125–35.
[21] Peace GS. Taguchi method: a hands-on approach. Reading, MA: Addison Wesley; 1993.
[22] Lee H, Lee JH, Pharr GM. A numerical approach to spherical indentation technique for material property Evaluation. J Mech Phys Solids 2005;53:2037–69.
[23] Lee JH, Kim T, Lee H. A study on robust indentation techniques to evaluate elastic–plastic properties of metals. Int J Solids Struct 2010;47:647–64.
[24] Wortman JJ, Evans RA. Young's modulus, shear modulus, and Poisson's ratio in silicon and germanium. J Appl Phys 1965;36:153–6.
[25] Jaccodine RJ. Surface energy of germanium and silicon. J Electrochem Soc 1963;110:524–7.
[26] Lemaitre P. Fracture toughness of Germanium determined with the Vickers indentation technique. J Mater Sci Lett 1988;7:895–6.